Mechatronics and Automation Technology
J.-Y. Xu (Ed.)

doi:10.3233/ATDE231144

Simulation and Optimization of Scissors Mechanism of Electric Charging Bow

Jun WU[a], Hongqing LI[a], Peng HU[a], Pengfei YUAN[a], Bingyun JIANG[b,a,1] and A.W TIAKO YOUANI[a]

[a] *Wanbang Digital Energy Co., Ltd, Changzhou213000, China*
[b] *School of Mechanical Engineering, Zhejiang University, Hangzhou310027, China*

Abstract. To improve the charging bow scissor mechanism's operating performance, a parametric model of the electric charging bow scissor mechanism was established, the scissor mechanism's hinge point coordinates were parameterized, and the optimization algorithm was used to optimize the parameters with a lifting force of 5000N as the target. First, the optimized structural parameters are obtained after multiple iterations using the NLPQLP direct numerical algorithm; then, the strength and stiffness simulation of the optimized scissor mechanism is performed to meet the strength and deformation requirements; and finally, the constant amplitude load method is used to conduct fatigue analysis on the optimized structure. According to the optimization results, the maximum lifting force of the scissor mechanism in the electric charging bow is reduced by approximately 18%. The lifting force is compared to the lifting force collected by the sensor, which verifies the structural optimization's effectiveness. Simultaneously, strength and stiffness simulation analysis determines the mechanism's material and processing technology, while fatigue analysis provides the foundation for subsequent life optimization. The modeling and analysis process used is simple and reliable and it has some engineering practical value.

Keywords. Charging bow; Scissors mechanism; Dynamics; Optimization; Simulation.

1. Introduction

The hydraulic cylinder is frequently used in the current scissors mechanism study to realize a rated load of features [1]. The kinematic and kinetic simulations are carried out using MATLAB/Simulink [2]. Furthermore, the dynamic motion of the scissors mechanism deployment in space with a self-balancing moment is calculated, followed by a check of the frame's stress and deflection [3]. Other spatial scissor mechanisms can be converted by actuators between arch-like, dome-like, and double curved geometries, where they can stabilize and carry loads [4]. In the industry, the scissor mechanism [5-7] is commonly used. By adjusting the position of the internal rotating joint via a primary scissors mechanism, an unequal-length scissors mechanism [8] is proposed. An elastically loaded scissors mechanism is employed in the creation of lightweight limbs for multi-legged robots. Simulations show that the suggested technique yields faster motion and greater output displacement [9]. The scissors mechanism is ideal for charging

[1] Corresponding Author, Bingyun JIANG, PhD, senior engineer, engaged in digital design and intelligent simulation, School of Mechanical Engineering, Zhejiang University, China; E-mail: bingyun.jiang@zju.edu.cn.

bows because it is simple to use and maintain [10]. As a result, it is vital to investigate the force and power of the scissors mechanism in order to meet specific operating requirements.

This paper will use an electric bus as a research object. Following the establishment of the scissors mechanism's parametric model, the optimization algorithm is used to obtain optimized rod length based on the target value of the hydraulic push rod lifting force, as well as the ideal position of the scissors mechanism's hinge point. Second, the appropriate material is chosen based on the strength analysis of the ultimate working conditions, and the charging bow structure is optimized and improved.

2. Virtual Prototype of Electric Charging Bow Scissors

2.1. The Model and Working Principle of Scissors Mechanism of Electric Charging Bow

Figure 1 represents the charging bow's bow end structure schematic diagram. The device's core consists of a hydraulic push rod and a four-stage rod group. Each stage is divided into two rows of scissors that are joined together by horizontal aluminum bars. A flexible rotating body assembly connects the bottom of the class IV rod group to the copper bar at the bow's end. All levels of rod groups are hinged at the first and last ends, and the connecting rod is hinged through the middle position in each stage. The hydraulic push rod 2 is fixedly connected with the bow head frame assembly 1, and the other side is connected with the main shaft via the electric push rod installation block in the first position of the class I rod group.

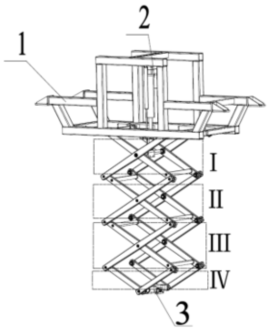

1. Bow head frame assembly ; 2. Hydraulic putter ; 3. Flexible rotating body assembly

Figure 1. Schematic diagram of the bow end structure of the charging pantograph.

2.2. Virtual Prototype of Electric Charging Bow Scissors

Since the modeling of the pantograph end device of the flexible rotating body assembly is complex, it is imported into ADAMS from external structure software, which allows the model size to be consistent and the accuracy of the model assembly to be highly reliable. The pantograph model end mechanism exported in CREO is shown in figure 2 (a). Figure 2 (b) depicts the position of each hinge point of the pantograph scissors mechanism.

(a) (b)

Figure 2. Charging bow end virtual prototype and mechanism schematic.

3. Modeling and optimization of Scissors Mechanism of an Electric Charging Bow

3.1. Design Variable

To achieve the purpose of rising and falling of the pantograph's scissors mechanism, the intermediate shaft is raised and lowered in the studied pantograph, so the pantograph should not only meet the lifting height requirements but also improve the lifting force of the hydraulic push rod, so the coordinates of each hinged point are taken as design variables for carrying out parametric design. A rotating pair is attached between the rod and the rod, a moving pair is attached to the push rod, and a speed drive is attached to the moving couple, with the speed set to 36mm/s. Furthermore, because the bottom of the bow end must also be arranged with copper bars, an 80kg weight is applied at the bottom to restore the accurate model. Finally, the design Variable is used to create the DV_1~ DV_6, and the resultant value is set to the maximum lifting force, as shown in equation (1).

$$maxF(x) \tag{1}$$

Where x is design variable， it represents DV_1 to DV_6.

Table 1. Parametric coordinates of the hinged points of the pantograph

Hinged points	X coordinate	Y coordinate	Z coordinate
A1	x0	-DV_1	-DV_2
A2	x0	-DV_1	DV_2
B1	x0	-DV_3	-DV_4
B2	x0	-DV_3	DV_4
C1	x0	-DV_5	-DV_4
C2	x0	-DV_5	DV_4
D1	x0	-DV_6	-DV_4
D2	x0	-DV_6	DV_4
E	x0	-(DV_1+DV_3)/2	0
F	x0	-(DV_3+DV_5)/2	0
G	x0	-(DV_5+DV_6)/2	0
H	x0	-(DV_1+DV3)/2-DV_6	0

Figure 2 (b) present the position of each hinge point of the pantograph scissors mechanism. θ is the angle formed by the rod and the z axis, with the fixed point of the hydraulic push rod serving as the coordinate origin. The YOZ plane charging pantograph's symmetrical structure is divided into front and rear lifting mechanisms. The hinge points of the grade I rod groups are A1, A2, B1, B2 (front) and a1, a2, b1, and b2 (back), respectively, in front of the negative direction of x. The class II pole group's hinged points are B1, B2, C1, C2 (front) and B1, B2, C1, C2 (back).

The grade I and II pole groups are linked by the B1, B2, b1, and b2 hinged points. The grade III pole group consists of C1, C2, D1, D2 (front) and c1, c2, d1, d2 (back). The C1, C2, c1, c2 connections connect the grade I and II pole groups. The hinged points of grade IV rod group are D1, D2 (front) and D1, D2 (back); they are linked to rod group III via these four hinged points. Only seven design variables DV_1~DV_6 must be established using the mechanism's coordinate system operation. Table 1 depicts the relationship between their coordinates.

3.2. Boundary Condition

Working specifications and performance criteria are controlled by charging standards in order to be as similar to the real motion process as feasible, hence the following restrictions must be met:

1) The distance between the top of the pantograph end and the back of the bus is greater than 1700mm, according to the stroke requirements of the mechanism at the end of the pantograph.

2) The preset θ range is from 5°to 55°, depending on the actual operation needs, the degree of complexity of the required lifting force change, and the overall layout requirements.

3) The mechanism stiffness should be evaluated when the charging bow is removed, according to the standard requirements. The y-direction height range is limited to 100mm.

4) To assure control cost, each variable's permissible fluctuation range is set to ± 10% of the initial value.

To obtain the best results, different combinations of the six variable settings listed above are tried. The NLPQLP optimization technique is used to optimize the lifting force of the charging bow's scissors mechanism as the optimization objective function, with a lifting power of 5000N as the aim, as stated in formula (2).

$$min\ (max\ (F(x_1, x_2, \dots \dots x_6) \tag{2}$$

Figure 3 illustrate the entire optimization process diagram. When the algorithm-filtered data is simulated, if the operation is abnormal, the result is skipped directly, making the process of obtaining the optimal goal an efficient one.

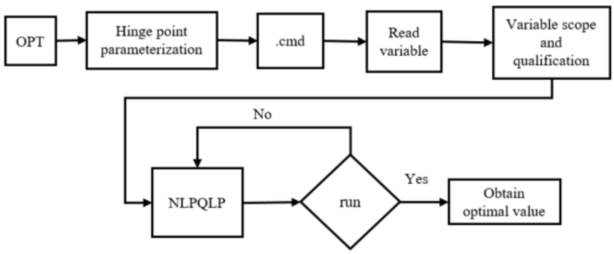

Figure 3. Optimized process.

3.3. Parameters Comparison before and after Optimization

Through the algorithm optimization of the maximum lifting force obtained from each operation, the number of iterations is shown in figure 4.

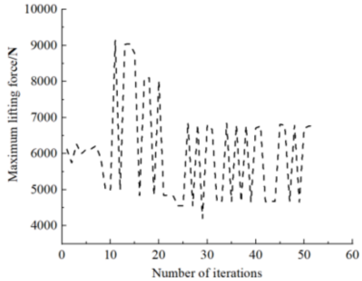

Figure 4. Number of iterations.

Subsequently, the coordinates of the hinged points of each rotating pair are obtained after the optimization iteration when the minimum value of the maximum lifting force is 4208.8N. The length of each rod is calculated using formula (3).

$$l = \sqrt{(x_2 - x_1)^2 + (y_2 - y_1)^2 + (z_2 - z_1)^2} \tag{3}$$

l represents the length of the rod in millimeter(mm), (x_1, y_1, z_1) and $(x_2, y_2, z_2)$are the three-dimensional coordinates of the two ends of the corresponding rod, respectively. The final calculated rod length parameters are shown in table 2.

Table 2. Comparison of each connecting rod length before and after optimization

Rod	Pre-optimization length /mm	Optimized length /mm	Rate of change/%
I	720	700	-2.78
II	720	700	-2.78
III	720	700	-2.78
IV	380	350	-7.89

Figure 5-7 presents the motion law and stress of the hydraulic push rod at the end of the charging bow before and after optimization, as well as the stress curve of each hinge point.

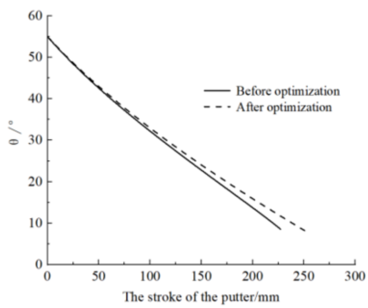

Figure 5. Diagram of the movement of the push rod before and after optimization.

Figure 5 shows that due to the connecting rod before optimization being longer than after optimization, the stroke of the push rod after optimization is less compared to prior optimization, which decreases by about 10.9%, indicating that the optimization effect is significant. Figure 6 depicts the force prior to and following optimization of the push rod, demonstrating that the lifting force before optimization increases sharply to

5146.19N during tightening, while the lifting force following optimization drops by approximately 18.2%. Given that the larger the push rod stroke is, the harder the operation of the entire mechanism is, and the greater the force is, the smoother the lifting force is shortly after optimization, decreasing the impact on the device.

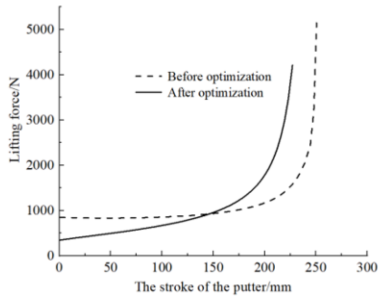

Figure 6. Diagram of the lifting force of the push rod before and after optimization.

Figure 7 presents the force of the hinged point A1A2~D1D2 prior to and subsequent to push rod stroke optimization; the force following optimization has been reduced compared to the force prior to optimization, and the force curve is smoother.

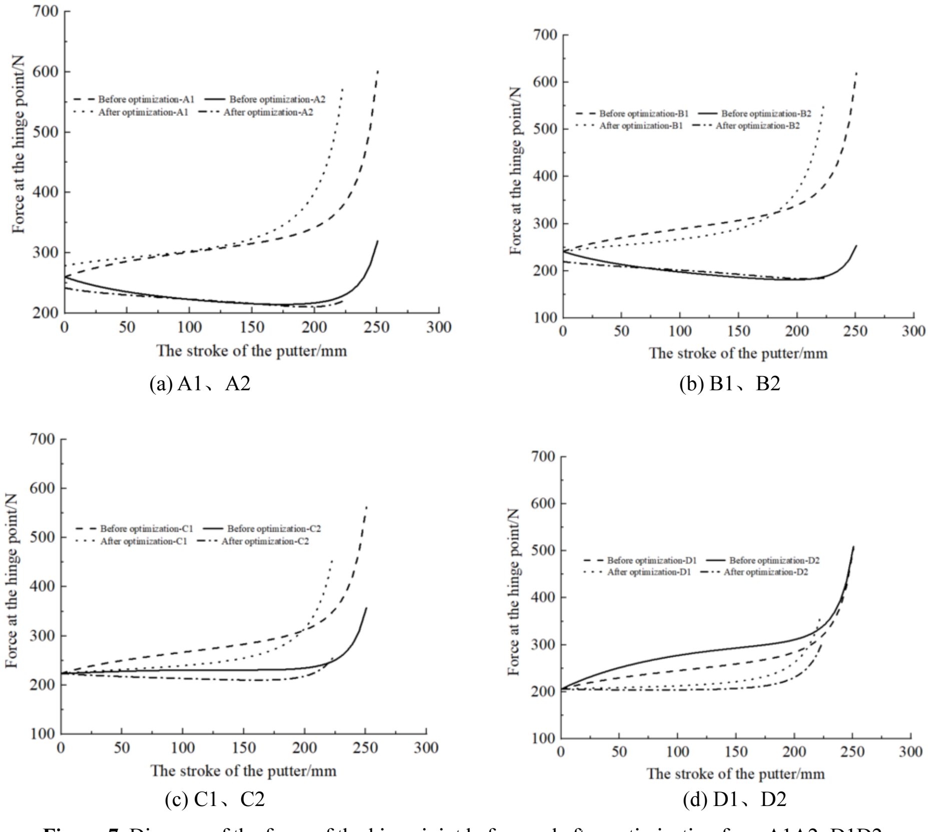

Figure 7. Diagram of the force of the hinge joint before and after optimization from A1A2~D1D2.

4. Extreme Conditions Finite Element Simulation

4.1. Strength Simulation Results

The optimized rod length parameters are obtained by optimizing the bar length of the scissors mechanism. The rod thickness is chosen based on the optimization and the strength of the optimized rod is analyzed. Preliminary rod materials are Al6063-T6 welding technology and Al6061-T6 solid machining technology. Table 3 shows the material properties of both materials.

Table 3. Alternative materials list

Material	Density/(t/mm^3)	Young's modulus/(MPa)	Yield strength /(MPa)	Tensile strength/(MPa)
Al6063-T6	2.7E-9	69000	215	240
Al6061-T6	2.7E-9	69000	275	310

When θ is 30 °, the two schemes of solid rod and 3mm hollow rod are used to analyze and compare the stress. When welding technology is used at the hinge of a 3mm hollow rod, the actual material strength should be judged by 60% of the yield strength. Machining technology is used for a rigid connecting rod, and the actual material strength should be judged by 80% of the yield strength.

Figure 8 shows that the maximum stress of the welding technology is approximately 214.76MPa when θ is 30°, which is located at the welding area, it has exceeded its yield strength and is easy to produce permanent deformation. Given that the machining technology's stress is less than the yield strength of the material, the yield risk is minimal.

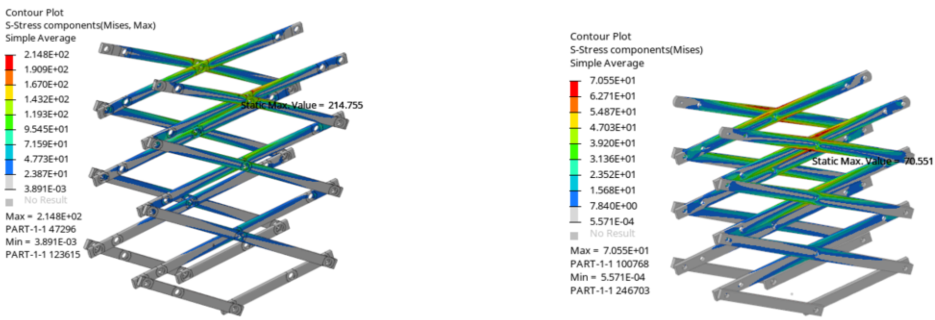

Welding technology Machining technology

Figure 8. Diagram of different processing stress at θ=30°.

For the scissors mechanism's connecting rod, the shorter the shaft, the bigger the lifting force, and the higher the force of the connecting rod. As a result, the Al6061-T6 material is employed and machined. When θ is 0°, the stress distribution of the connecting rod using the machining method is computed, as shown in figure 9, and the stress is around 152.30MPa, which is less than the material's yield strength. It is suggested that this material can be employed as the connecting rod of the scissors mechanism to fulfill the strength requirements.

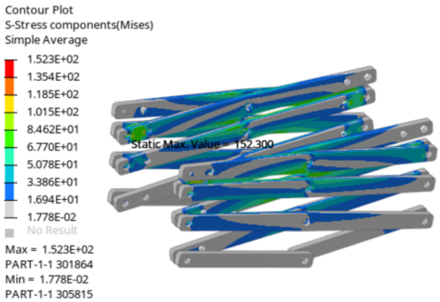

Figure 9. Diagram of machining technology stress at θ=0°

4.2. Stiffness Simulation Results

The material and processing method are decided by optimizing the strength of the scissors mechanism. Given that the top of the scissors mechanism must be in the shell following gravity action, the stiffness must also fulfill specific requirements. For stiffness simulation, different bar thicknesses are chosen so that the sagging height is less than 100mm.

Figure 10 and figure 11 illustrate the displacement behind the top of the scissors mechanism for 20mm and 30mm rod thicknesses, respectively. The downward deflection of the lowest scissors is the most severe, and the displacement of the 30mm thick rod is nearly half that of the 20mm thick rod, meeting the requirement that the scissors mechanism is completely covered inside the rechargeable bow cover shell after the work is completed.

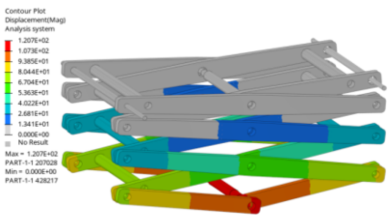

Figure 10. Displacement of 20mm thickness.

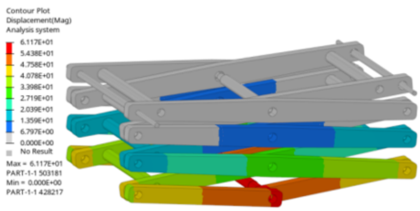

Figure 11. Displacement of 30mm thickness.

4.3. Fatigue Simulation Results

The self-defined material curve is employed in the nCode to match the S-N curve of Al6061-T6, as illustrated in figure 12. The scissors mechanism is next subjected to a stress fatigue simulation examination. Since the frequency is less compared to the frequency of the general mechanism, a static fatigue simulation of the scissors mechanism that received the top is performed, and the constant amplitude load (1, -1) curve is utilized to provide the life cloud diagram of the bar, as shown in figure 13.

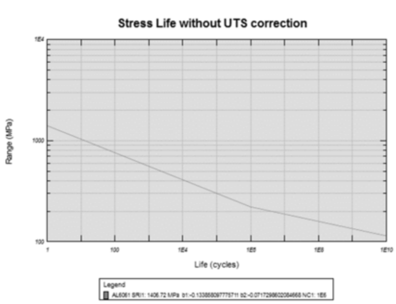

Figure 12. S-N curve of Al6061-T6.

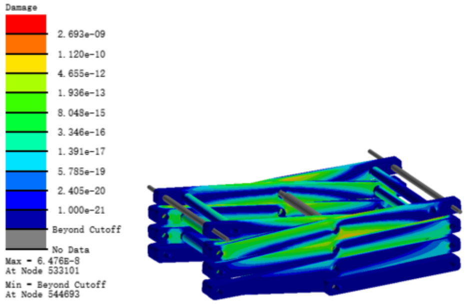

Figure 13. Life cloud map of the rod

Figure 14 shows that the maximum fatigue damage value at the first grade hinge is 2.69e-9, which approaches infinite life, suggesting that the structure satisfies the criteria of engineering design and operation.

5. Test

The improved charging pantograph is proofed after the aforementioned optimization findings and strength analysis, and the final structural characteristics are provided in table 4.

Table 4. Structure parameter

Rod	Length/mm	Material	Thickness/mm
I/II/III	700	Al6063-T6	30
IV	350	Al6061-T6	30

Sensors are fitted on the bow head frame, as illustrated in figure 14 and figure 15, to monitor the lifting force of the hydraulic push rod, eliminate outliers, fit the data, and compare it to simulation data.

Figure 16 shows that once the hydraulic rod is lifted, the force trend is steady, but the sensor test result is excessively high, owing to the simulation ignoring the friction between the hinges and the gravity of the rod.

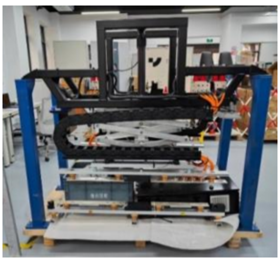

Figure 14. Actual product.

Figure 15. Charging bow end sensor.

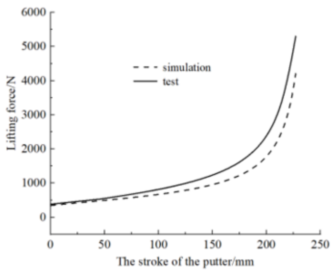

Figure 16. Comparison diagram of simulation and test of lifting force.

6. Conclusion

The dynamic modeling of an electric charging bow has been done in this research, and the hinge point coordinates are parameterized. Optimization software optimizes. The target lifting force, and the ideal rod length parameters and lifting force are determined.

The improved scissors mechanism's strength and stiffness are simulated using various materials and production processes. The materials and manufacturing processes are chosen based on the results of the stress and displacement simulations, as well as the rod thickness is calculated.

The fatigue simulation of the scissors mechanism is performed, which serves as the foundation for eventual fatigue life optimization. A lifting force test is performed on the produced prototype to validate the optimization results.

Acknowledgements

Project fund: Jiangsu Province major common technology research and development-High Power Automatic Charging System (GC04C200001) and the 15th batch of Changzhou Science and Technology Plan (CZ20210009)

References

[1] Hongyu T, Ziyi Z. Design and simulation based on pro/e for a hydraulic lift platform in scissors type [J]. Procedia Engineering. 2019. DOI:10.1016/j.proeng.2011.08.1153.
[2] Tao Liu, Jian Sun. Simulative Calculation and Optimal Design of Scissor Lifting Mechanism [J]. IEEE Industrial Electronics, 2009:682-685.
[3] Takatsuka M, Ohmori H. Dynamic Structural Analysis of Deployment of Scissors Structure in Space [J]. International Journal of Space Structures, 2013, 28(1):1-14.
[4] Akgün, Y. et al. A novel adaptive spatial scissor-hinge structural mechanism for convertible roofs [J]. Engineering Structures, 2011, 33(4), 1365–1376.
[5] Gao Zhao. Design and optimization of scissor lift system [D]. Shandong University of Science and Technology, 2018.
[6] PETRU M, SEVCIK L, MASIN I, et al. Dynamic analysis of lifting platform construction for car relocation [J]. Modern Methods of Construction Design, 2014, 8:517-524.
[7] Wei Zhang, Chao Yan. Optimization design of input location parameters of scissor lift mechanism [J]. Key Engineering Materials, 2016, 693: 163-168.
[8] Bo H, Xiangkun L, Jian S, et al. Design and dynamic analysis of a scissors hoop-rib truss deployable antenna mechanism [J]. Defence Technology, 2023, 24.
[9] Nizami, M. H. A. et al. Proximal Actuation of an Elastically Loaded Scissors Mechanism for the Leg Design of a Quadruped Robot [J]. IEEE Access, 2020, 8:208240–208252.
[10] Teng Zhao, Yuanqiang Wang, Jiangfeng Ji. Research on the Development Status of Aerial Work Platforms [J]. Construction Machinery Technology & Management, 2020, 33(01):93-94.